Int. J. Heat Mass Transfer. Vol. 33, No. 1, pp. 29–38, 1990
Printed in Great Britain

0017–9310/90 $3.00 + 0.00

Microscopic study of coupled heat and mass transport during unidirectional solidification of binary solutions—I. Thermal analysis

SOHRAB KOUROSH

Department of Orthopaedic Surgery, The University of Texas Health Science Center at Dallas, Dallas, TX 75235, U.S.A.

and

MICHAEL E. CRAWFORD and KENNETH R. DILLER

Department of Mechanical Engineering and Biomedical Engineering Center, The University of Texas, Austin, TX 78712, U.S.A.

(*Received* 27 *December* 1988 *and in final form* 20 *April* 1989)

Abstract—Coupled heat and mass transport phenomena occurring during the unidirectional solidification of a binary solution are studied utilizing a specially designed freezing stage for transmitted light microscopy. The apparatus provides the capability for real time direct observation of the freezing process along with simultaneous measurement of the time evolution of cellular-scale coupled concentration and temperature fields and their interaction. The experimental data provide a comprehensive specification of a freezing process at the microscopic level for use in developing models of the binary solidification process, including temporal and spatial temperature profiles, local rates of cooling and heat flux, and interface velocity and temperature.

INTRODUCTION

COUPLED heat and mass transport phenomena play a governing role in the solidification of binary alloys and solutions. A majority of the analytical studies on solidification have been effected on a macroscopic scale utilizing simplifying assumptions such as zero subcooling, homogeneous and instantaneous solute distribution within the solid and liquid phases and pure or eutectic chemical composition. Many of these assumptions may seem justifiable when the system is considered at the macroscopic level, but this is not the case when the process is evaluated on a microscopic scale. Nonhomogeneities occur in the system due to spatial distribution of boundary condition, asymmetrical lateral segregation, non-equilibrium freezing conditions at the interface, and constitutional supercooling. These affect the geometry of the thermal field and the morphology of the interface, and thus the microstructure of the solid phase, all of which are observable only at the microscopic level.

The importance of microstructure in determining the physical characteristics and properties of solid solutions makes it clear that a rigorous, rational macroscopic understanding and control of the solidification process would be greatly enhanced if the kinetics of the process were understood at the microscopic scale, given that macroscopic phenomena may be considered a cumulation of microscopic-scale events. As an example, in the cryopreservation of living cells and organs, the overall response of tissues to freezing trauma is mediated by the interaction between individual cells and their immediate microenvironment. Consequently, microscopic-scale nonhomogeneities in the concentration and thermal fields may result in a large spatial differential in the survival of cells within a given system for a single freezing protocol defined at the boundary [1, 2]. Thus, quantitative analysis of the governing parameters is directly attendant to the basic understanding of the full-scale freezing problem.

Few experimental and analytical studies of freezing at the microscopic level have been carried out. In recent years a theoretical study by O'Callaghan and Cravalho [3, 4] addressed the description of thermal and concentration fields for planar and cellular morphologies. Körber *et al.* [5, 6] investigated solute redistribution during freezing of binary aqueous salt solutions. Thermal and concentration fields were measured for planar and cellular morphologies.

The objective of the present investigation was to study microscopically the solidification process in a binary mixture the thermophysical characteristics of which simulate those of a physiological solution. Transient and steady-state heat and mass transfer data were obtained on a special freezing stage mounted on a light microscope, incorporating microthermocouples to monitor the transient temperature field, and utilizing digital densitometric analysis to quantify the evolving two-dimensional concentration field in front of the moving phase interface. Due to the extensive data acquired, numerous parameters that were evaluated, and unique aspects of the heat and mass transfer analyses, the study is

NOMENCLATURE

$A(t)$, $B(t)$, $C(t)$	curve-fit coefficients
k	thermal conductivity [W m^{-1} K^{-1}]
L	latent heat of fusion [J kg^{-1}]
t	time [s]
V_{th}	theoretical interface velocity [m s^{-1}]
x	distance in direction of freezing [m].

Greek symbol

ρ	solution density [kg m^{-3}].

Subscripts

if	interface
l	liquid phase
s	solid phase.

divided into two parts. The first, as reported herein, addresses the analysis of the thermal data for a typical experiment which produced a cellular-shaped interface, including validation of the data and the quantitative relationship among the thermal parameters and the interface velocity and morphology. The second part, to be reported in a companion paper [7], concerns analysis of mass diffusional data and its relationship to the interfacial and thermal parameters, along with analysis of constitutional supercooling phenomena.

EXPERIMENTAL APPARATUS AND PROCEDURE

Experiments were carried out on a specially-designed low-temperature stage mounted on a Zeiss Universal light microscope equipped for simultaneous monitoring of image and temperature data [8]. The system provides capabilities for real time observation of the freezing process, including the temporal evolution of the interface position and its morphology, while simultaneously recording the time-dependent temperature and concentration fields.

Design of the cryomicroscope stage and the integrated total apparatus are shown in Fig. 1, which depicts the side and plan views of the stage and a cross-section of the freezing chamber. In the freezing chamber a liquid specimen is solidified as a quasi one-dimensional sheet. The freeze front moves left to right, i.e. normal to the direction of the smallest specimen dimension, which corresponds to the optical axis of the microscope, between two copper blocks which serve as a heat sink and heat source. The upper and lower surfaces of the specimen are insulated by laminated multiple-pane window covers, thereby constraining the heat flux to flow in the specimen unidirectionally between the source and sink. Transient thermal boundary conditions were modulated by varying the sink temperature, whereas the source temperature was fixed at near-ambient conditions. Details of the stage design and operating characteristics have been presented and discussed previously [8].

To execute an experiment, the stage was mounted on the microscope and illuminated with transmitted light using a halogen lamp and brightfield condenser. Approximately 4 μl of specimen solution was deposited into the freezing chamber under the upper laminated cover window, and the data acquisition equipment was activated. A flow of refrigerated dry nitrogen vapor from a shell-and-tube liquid nitrogen heat exchanger was directed through a manifold in the copper heat sink to commence cooling at one end of the specimen chamber. The flow was regulated according to a preprogrammed protocol, and the process was monitored and controlled either using a microprocessor-based temperature controller [9] or manually. The design characteristics of the stage produced a solidification process that proceeded in a unidirectional pattern across the microscopic field of view, with the temperature field symmetric about the primary axis defined by the direction of the freeze front, as demonstrated in ref. [8].

Four types of data were recorded as functions of time and position during each experiment:

(a) temperature;
(b) solute concentration;
(c) interface position;
(d) interface morphology.

The temperature field was monitored by a linear array of seven microthermocouples embedded in the surface of the freezing chamber. These thermocouples are positioned in a staggered array at 2 mm intervals along the primary axis, displaced 2 mm on either side of the centerline of the chamber. The thermocouples were read sequentially at 6 s intervals and recorded on a Fluke Model 224 A/D Data Logger, which in turn formats and writes a digitized temperature record onto a Tektronix Model 4922 Digital Cassette Tape Recorder for future data analysis.

Solute concentration measurements were obtained for a binary mixture using digital densitometric analysis of sequentially recorded micrographs, as discussed in detail in the companion paper [7]. The mixture used in the experiments was a 2.16 wt% aqueous solution of sodium permanganate, chosen to simulate the freezing of a physiological salt solution. The primary advantage of using sodium permanganate to form a salt solution is that it has a dark magenta color that enables local concentration to be measured densitometrically. In addition, the thermophysical properties relevant to heat and mass transport are very similar to those of sodium chloride, which is the solute of greatest physiological significance. Figure 2 shows

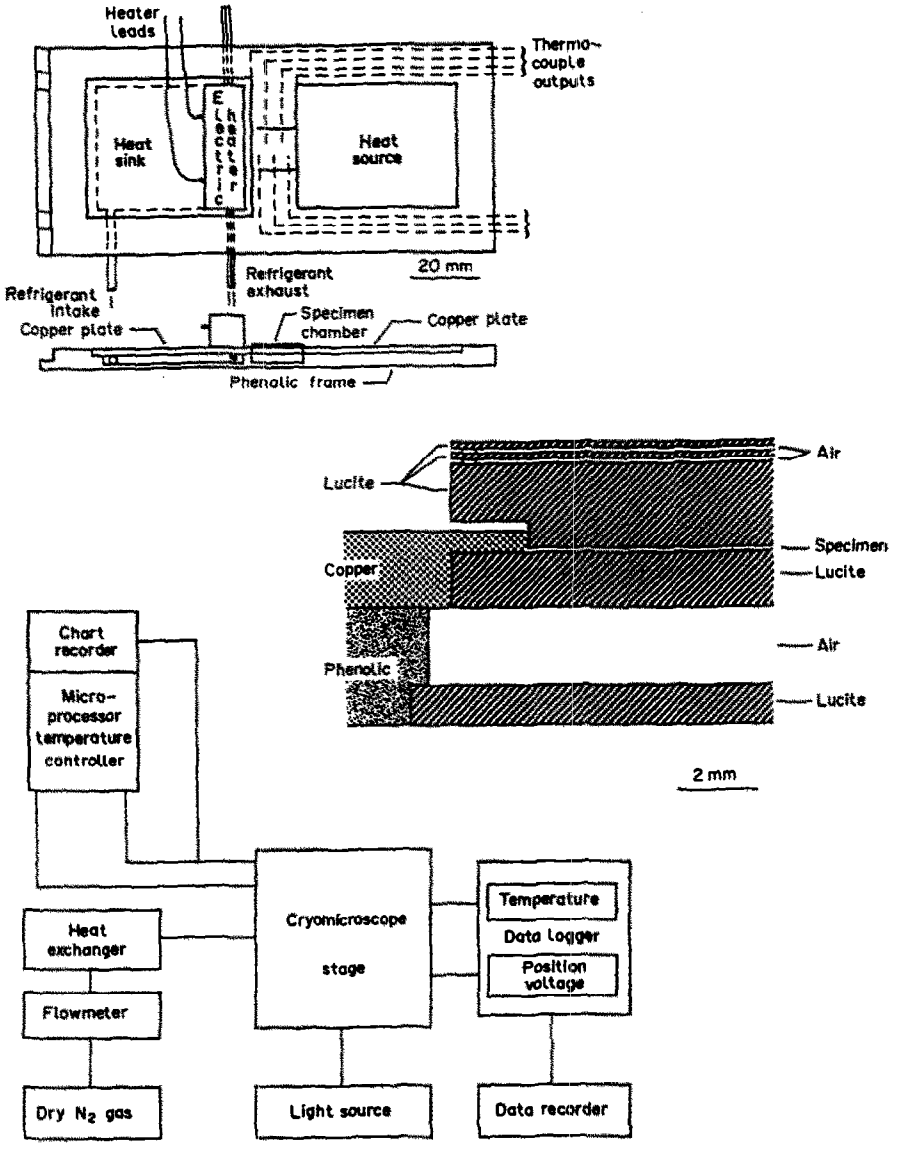

FIG. 1. Transmitted-light microscope freezing stage and experimental system for studying binary solidification processes.

the phase diagram for sodium permanganate, adapted from ref. [10]. The eutectic freezing point is $-15.8°C$. Table 1 gives pertinent thermophysical property values for the solution.

Movement of the phase interface was monitored with a linear position transducer mounted on the cryomicroscope stage. As the stage was manually traversed to keep the moving phase boundary centered within the field of view during freezing, the transducer output was recorded on the Data Logger. The position information was subsequently time-differentiated to determine the interface velocity. A 35 mm film camera and a video camera were mounted on the cryomicroscope to provide simultaneous film and electronic format recording of the dynamic freezing process, primarily to be used for offline mass transfer and interface morphology analysis. The measurement accuracies of the various parameters were assessed from calibration tests as follows: temperature, $\pm 0.5°C$; solute concentration, ± 0.1 wt% for nearly pure solvent to ± 2.5 wt% for near-eutectic states; and ± 0.01 mm for interface position for a typical cellular length of up to 100 μm and a cell spacing of about the same order of magnitude.

DATA ACQUISITION AND ANALYSIS

Data were obtained for approximately 30 controlled experimental trials characterized by cold-end boundary cooling ranges within the range from 0.5 to

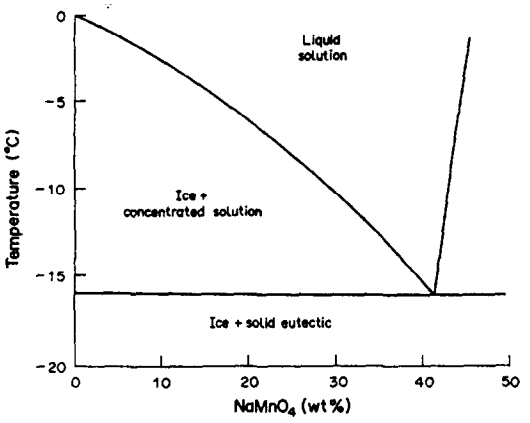

FIG. 2. Thermodynamic liquidus curve for aqueous sodium permanganate solution.

60°C min^{-1}, and with overall temperature limits from 25 to −100°C. Some protocols included periods of sub-zero isothermal boundary conditions. The analysis procedure for the resulting data is presented here and discussed for a single representative experiment composed of a mixed freezing protocol, including both steady-state and transitory boundary conditions.

Thermal data acquisition is accomplished by sequential readings of the thermocouple array embedded in the surface of the specimen chamber of the freezing stage. The temperature and position transducer voltages are digitized together on the Data Logger and recorded with a common time base on a magnetic tape for subsequent computer analysis. The algorithm performs the necessary data reduction and presents the results in convenient tabular and graphical formats.

The displacement transducer voltage, obtained at discrete time increments, is interpolated for 6 s intervals between consecutive readings to derive a continuous description of the phase interface position as a function of time. The transient behavior of the system is such that the sampling period is short compared with significant alterations to the position and velocity. Duration of a typical trial run was of the order of 30 min or more. A scale factor defined by calibration tests is used to convert the transducer voltage to a distance from the cold-sink end of the specimen chamber. A cubic spline is then curve-fit to the data to produce the desired displacement function, which can be differentiated with respect to time to estimate the instantaneous local interface velocity. A similar curve-fit procedure is used for temperature data to determine its time derivative, representing the local rate of cooling of each thermocouple.

The technique developed to determine the interface temperature for the one-dimensional freezing process required that the temperature distribution within the solid and liquid phases be approximated by analytical functions. Quadratic polynomials of the form

$$T_{\text{int}}(x,t) = A(t)\cdot x^2 + B(t)\cdot x + C(t)$$

were chosen, based on curve-fit analysis of thermocouple data for times when the freeze front passed above the various thermocouple positions. As the solid–liquid interface advances into the liquid phase, the position, slope, and curvature of the temperature profile change in time as a function of the boundary rate of cooling, but the profiles remain approximately parabolic. This fact was used to develop the method for estimating the interface temperature. Consider the time during the experimental trial when the interface is exactly above a thermocouple station. The polynomial coefficients A, B, and C are determined for the liquid phase using that thermocouple and the two immediately in front of it. With the next data scan, 6 s later, the interface has advanced forward. The predicted interface temperature is obtained using a modified $A(t)$ and the temperatures of the two thermocouples in the liquid phase adjacent to the interface. The value of $A(t)$ is obtained by subtracting a correction factor equal to the change in the furthermost of the two thermocouples divided by the square of its location. If the interface is within 0.05 mm of the next thermocouple, the interface temperature is found by backward extrapolation of a polynomial constructed from three thermocouples in the liquid phase.

The thermal gradient in the liquid phase is calculated by differentiating the quadratic temperature equation with respect to position and evaluating it at the interface position. The temperature gradient in the ice phase is determined by constructing a quad-

Table 1. Physical properties of the freezing medium

Mass diffusivity of liquid	D_l	1.25×10^{-9} m^2 s^{-1}
Thermal diffusivity of liquid	k_l	0.603 W m^{-1} K^{-1}
Thermal conductivity of solid	k_s	2.22 W m^{-1} K^{-1}
Thermal diffusivity of liquid	α_l	1.44×10^{-7} m^2 s^{-1}
Thermal diffusivity of solid	α_s	1.15×10^{-6} m^2 s^{-1}
Heat capacity of liquid	c_l	4.186×10^3 J kg^{-1} K^{-1}
Heat capacity of solid	c_s	1.950×10^3 J kg^{-1} K^{-1}
Surface energy	γ	2.6×10^{-2} J m^{-2}
Latent heat of fusion	L	3.33×10^5 J kg^{-1}
Entropy	ΔS	-1.22×10^{-6} J m^{-3} K^{-1}
Initial solute concentration	C_∞	2.16 wt%
Equilibrium phase-change temperature of initial solution	T_m	272.6 K

ratic polynomial using the interface temperature and data from two thermocouples in the solid phase and differentiating it with respect to x. The position of the equilibrium freezing temperature isotherm (-0.532°C for the 2.16 wt% aqueous solution) is calculated from the ice-phase polynomial.

Data reduction procedures to determine the interface temperature were verified by two independent tests. First, the interface temperature was predicted by the model for the times that the freezing front was passing a microthermocouple location where it could be measured directly. Comparison of the predicted and measured temperature values was always within the temperature uncertainty estimate. The second validation test is described in the following section.

RESULTS AND DISCUSSION

The measured time–temperature records of the microthermocouples for the representative experimental trial are presented in Fig. 3. Also depicted in the figure are the microthermocouple locations in the freezing chamber. The lowest temperature curve, #1, is obtained from the thermocouple embedded under the edge of the chamber at the thermally-controlled boundary, and the upper curve, #7, is measured at the opposite end of the chamber where there is a free-floating warm boundary condition. The temperature plot for station 1 defines the freezing protocol, which consisted of a combination of constant rate cooling, steady boundary state, and a transitory cooling mode. The calculated interface temperature curve is also shown in Fig. 3, depicted by the stars. The discontinuity in the interface temperature curve near the beginning of the trial results from an initially large supercooling of the solution prior to the nucleation of ice, followed by a local temperature increase as latent heat is released more rapidly than it can be conducted away.

Local rate-of-cooling plots for these same thermocouple stations are shown in Fig. 4. The change in thermal boundary condition midway into the trial is seen as a sharp increase in cooling rate. These curves illustrate clearly the damping of modulations in the boundary condition due to increasing cumulative thermal capacitance at points progressively further to the interior of the system.

In Fig. 5 the experimentally determined position of the solid–liquid interface is plotted as a function of time, along with the computed temporal position of the equilibrium phase-change isotherm for the initial liquid solution composition (-0.53°C). The curves are parabolic in shape for the initial and subsequent (starting at about 1200 s) constant cooling rate portions of the freezing protocol. Changes in the slope and curvature in the curves are correlated with transitions in the boundary conditions. The parallel portions of the two curves in Fig. 5 describe regions of steady growth of the interface, which implies an approximately constant interface velocity. The separation distance between the curves, referred to as constitutional supercooling, can be related to the solute concentration at the interface through the system phase diagram. At the beginning of freeze-front growth the separation is due to the initial solution subcooling, and subsequent to nucleation the interface velocity increases until a steady state is attained. During the transition period when the cooling rate at the boundary is suddenly increased, the distance between the two curves becomes larger. This increased separation is partly due to a depression of the equilibrium solidification temperature caused by a higher interface solute concentration. Another contributing factor is a transient interface morphology for which

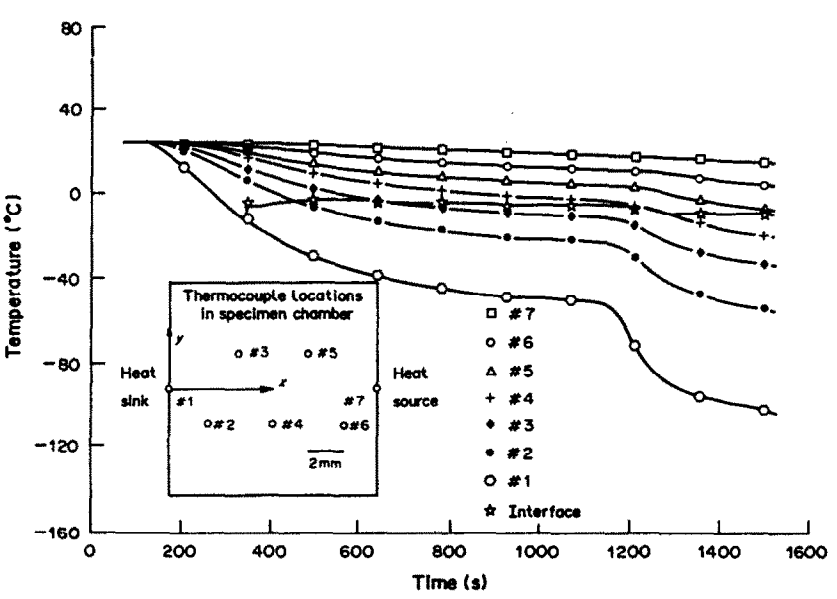

FIG. 3. Microthermocouple temperature–time history for a medium–slow freezing protocol.

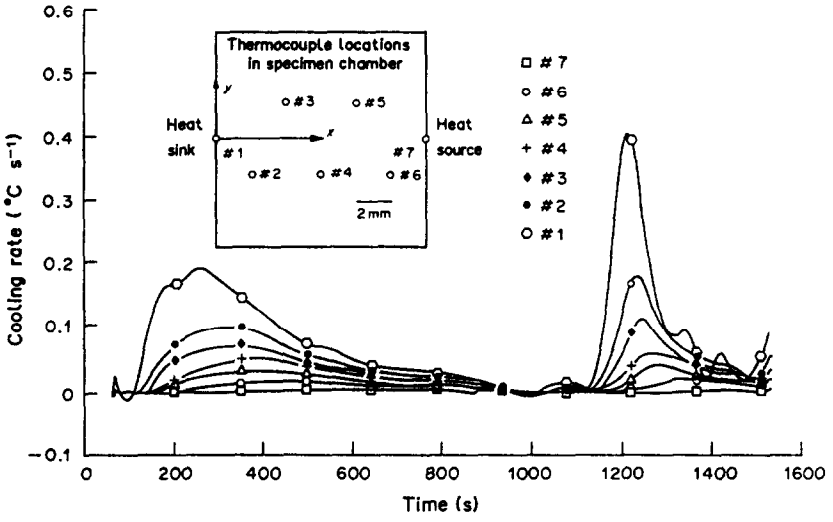

FIG. 4. Microthermocouple rate-of-cooling profiles for the medium–slow freezing protocol.

a tip of a growing cell may become thinner as it advances at a more rapid rate than the basal plane of the cells. Thus, during the transition period the latent heat removal associated with movement of the interface tip is less than if solidification were occurring uniformly throughout the two-phase region, and the interface velocity is temporarily increased disproportionately to the heat flow.

The solid–liquid interface is in the vicinity of the cellular tips. It should be noted that the cellular morphology, as depicted in Part II [7], contains a fairly deep intercellular region, the overall dimensions of which are of the order of 100 μm long with a spacing of about 100 μm between tips. Within this intercellular region there was no optical differential between solid and liquid phases, nor was the eutectic temperature front detected. Thus it was not possible to distinguish the colder vitreous phase in this region to identify a clearly defined basal plane.

The classical Neumann analysis of the freezing process predicts that under steady-state conditions the interface position should be a function of the square root of time. The experimental data is plotted according to this relationship in Fig. 6 with the result that approximately linear behavior results for the two portions of the protocol having nearly steady boundary conditions. Agreement between the data and the simple model is surprisingly good in the light of the transitory nature of the trial and deviation of the system from ideal one-dimensionality. A prior finite element analysis of the temperature distribution through the specimen and LUCITE substrate of the microscope stage showed that the maximum temperature variation along the optical axis is no greater than a few tenths of a degree for typical cooling protocols [8]. Thus, conjugate thermal effects between the specimen and the stage should produce no significant effect on comparison of the experimental data with the classical Neumann analysis.

Figure 7 shows the experimentally determined interface velocity vs time for this medium–slow freezing protocol. Before solidification begins, the velocity is zero, and the onset of nucleation produces the largest velocity, partly influenced by the initial subcooling of

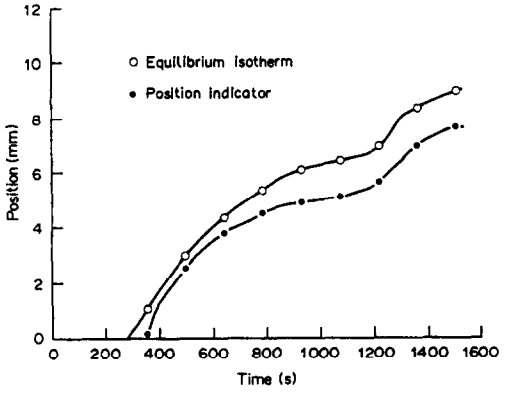

FIG. 5. Comparison of equilibrium and experimentally determined solid–liquid interface advancement.

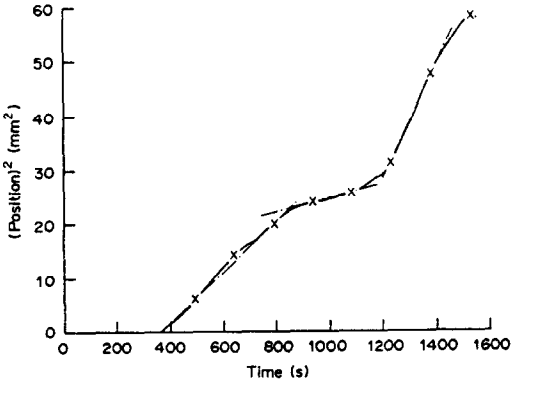

FIG. 6. Confirmation of a Neumann type of advancement of the solid–liquid interface.

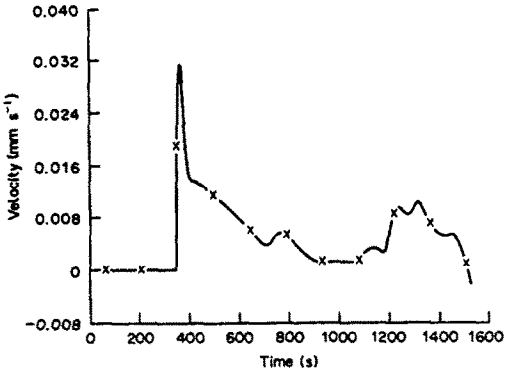

FIG. 7. Velocity of the solid–liquid interface during advancement.

the liquid. The velocity basically follows the boundary cooling rate depicted by curve #1 in Fig. 4, with the velocity approaching zero as the boundary cooling rate drops off and the protocol becomes one of a near-constant sub-zero holding temperature (see Fig. 3). The initiation of a new boundary cooling rate, about 1200 s into the trial, is seen in Fig. 7 as an increase in interface velocity.

An assessment of the accuracy of the computational procedure for calculating interface parameters can be made by comparing calculated first-law interface velocity values to the experimentally determined values. The assumption is that the analytical determination of the temperature profiles in the solid and liquid phases leads to the correct temperature at the interface. An energy balance is applied at the phase boundary to predict the interface velocity based on the differential between heat diffusion in the solid and liquid phases, which could then be compared with the measured value. The velocity V_{th} is calculated by

$$V_{th} = \frac{1}{\rho L}\left[k_s \frac{\partial T}{\partial x_{s,if}} - k_l \frac{\partial T}{\partial x_{l,if}}\right]$$

where L is the latent heat of fusion, ρ the solution density, and k_s and k_l the thermal conductivities of the solid and liquid phases. The thermophysical properties are those appropriate to the interface temperature, and thus become insensitive to variable property effects associated with temperature gradients in the solid and liquid phases. The experimental uncertainty associated with the interface velocity calculation is addressed in ref. [8] and determined to be ± 0.01 mm s^{-1}.

This procedure was first tested using analytical data derived from a Neumann analysis as an experimental data set [11]. The analysis is that for the solidification of pure water resulting from a step-temperature change at the boundary. The analytical solution provided temperature–time values for positions corresponding to the seven microthermocouple locations on the cryomicroscope stage. These are plotted in Fig. 8. Curve #1 shows the freezing protocol, which was the step-change constant boundary temperature from 4 to −4°C. These data were then processed with the experimental data-analysis procedure to calculate temperature profiles in the solid and liquid phases, rate-of-cooling profiles, and the interface temperature and velocity, and the results were compared with values for the exact solution.

The variation between the computed and exact Neumann values of the interface temperature is shown on Fig. 8. This calculation, using the quadratic poly-

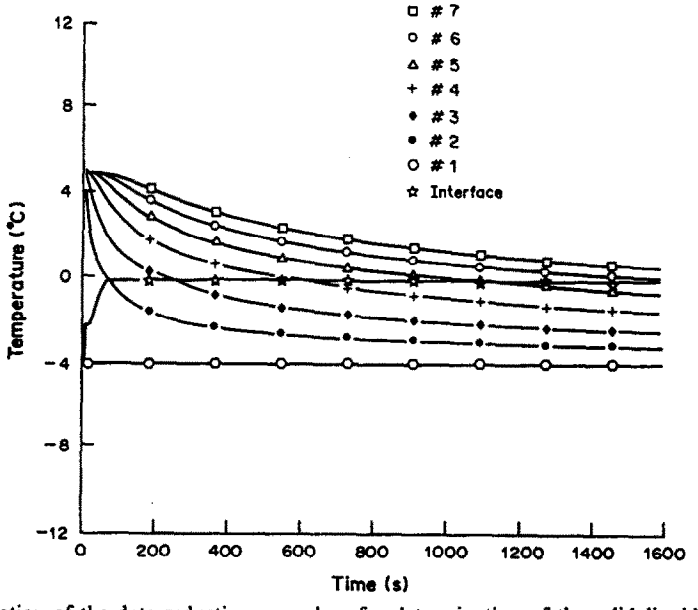

FIG. 8. Validation of the data reduction procedure for determination of the solid–liquid interface time history using a temperature–time field generated from the classical Neumann freezing problem.

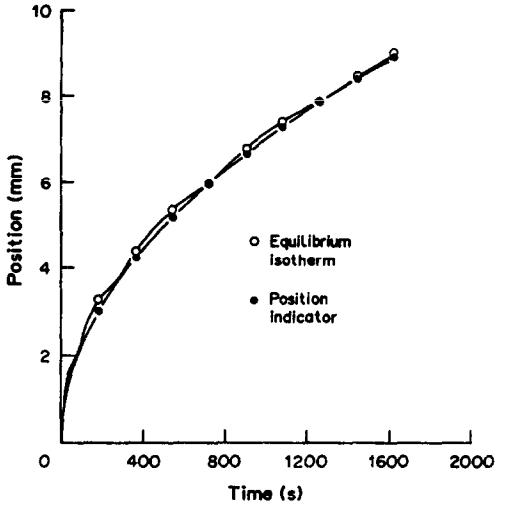

FIG. 9. Validation of the procedure for calculating the solid–liquid interface advancement for the Neumann temperature distribution.

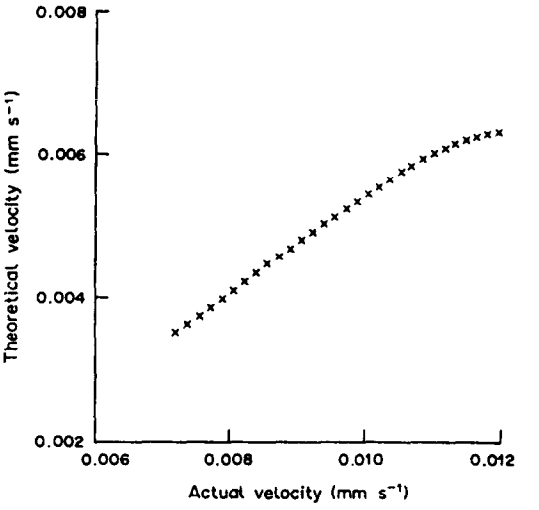

FIG. 11. Comparison of the energy-balance calculated interface velocity with the experimentally determined value for the medium–slow freezing protocol.

nomial technique that adjusts $A(t)$, is the least accurate of the computed parameters. The deviation from theory was within $\pm 0.01°C$. Figure 9 shows the position vs time plots of the interface, from the analytical solution, and the equilibrium isotherm, as an output of the data analysis procedure. Recall that the equilibrium isotherm is used in assessing the constitutional supercooling of the system. The close match of these two curves indicates that the method for determining the position of the equilibrium isotherm is consistent with theory. The final test of the data-reduction procedure is to calculate the V_{th} distribution from the first-law analysis described above and compare it with the Neumann-solution interface velocity distribution. Figure 10 shows the comparison, which would theoretically plot as a line 45° to the abscissa. Deviation from the line is $\pm 2\%$.

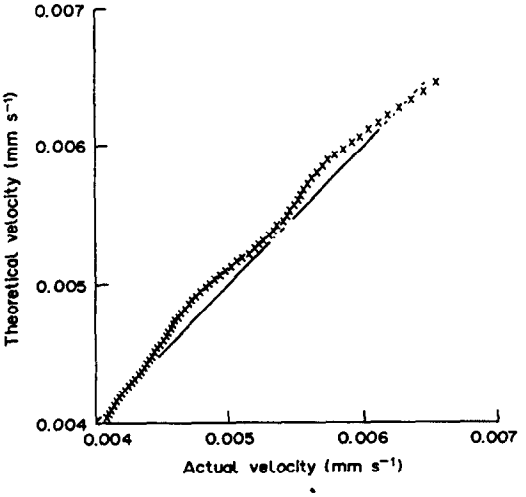

FIG. 10. Validation of the procedure for calculating the solid–liquid interface velocity for the Neumann temperature distribution.

Figure 11 presents a plot of the calculated interface velocity for the quasi-steady-state part of the freezing experiment vs the actual measured velocity. Values for the thermophysical properties of the solution are given in Table 1, with the density of the sodium permanganate solution obtained by interpolating values given in ref. [10]. The plot does not show a slope of unity, but it does plot as a straight line. While this could be attributed to uncertainties in the measurements or the thermophysical properties, the applicability of the first-law equation for the case of a non-planar interface is also a concern. The equation presented above assumes latent heat is released over a planar interface, and the experimental interface condition is one of a cellular interface. This suggests that the latent heat is proportional to the ratio of the solid-phase area to the planar area. Multiplication of the planar front first-law value by an experimentally determined area ratio, obtained as a part of the mass transfer part of the experiments, results in a near-unity, unshifted plot of first-law velocity vs experimentally determined velocity [7].

SUMMARY

An experimental facility has been designed to obtain data for the unidirectional solidification of binary solutions with solute exclusion from the solid phase. The system provides the capability for real time direct observation of the freezing process along with simultaneous measurements of the one-dimensional temperature field and the two-dimensional concentration field in the vicinity of the solid–liquid interface. The overall objective of the experiments is to provide a data base for the development of analytical models for predicting the freezing process and the interface morphology as a function of time. The ex-

perimental results contained in the paper are representative of the data base acquired with the facility. The data include the temporal and spatial temperature profiles, local rates of cooling and heat flux, and interface velocity and temperature. Internal consistency of the data is verified by comparing the interface velocity from physical measurements with an energy balance based on deduced temperature gradients in the vicinity of the solid and liquid phases at the moving boundary. The mass transport results and analysis of cross-coupling effects and constitutional supercooling are presented in a subsequent paper.

Acknowledgement—This research was sponsored by the National Science Foundation under Grant Nos. MEA-8023267 and CBT-8713600.

REFERENCES

1. B. Rubinsky and E. G. Cravalho, An analytical method to evaluate cooling rates during cryopreservation protocols, *Cryobiology* **21**, 303–320 (1984).
2. L. J. Hayes, K. R. Diller and H. S. Lee, Prediction of local cooling rates and cell survival during the freezing of cylindrical specimens, *Cryobiology* **25**, 67–82 (1988).
3. M. G. O'Callaghan and E. G. Cravalho, An analysis of the heat and solute transport during solidification of an aqueous binary solution—I. Basal plane region, *Int. J. Heat Mass Transfer* **25**, 553–562 (1982).
4. M. G. O'Callaghan and E. G. Cravalho, An analysis of the heat and solute transport during solidification of an aqueous binary solution—II. Dendrite tip region, *Int. J. Heat Mass Transfer* **25**, 563–573 (1982).
5. Ch. Körber, M. W. Scheiwe and K. Wollhover, Solute polarization during planar freezing of aqueous salt solutions, *Int. J. Heat Mass Transfer* **26**, 1241–1253 (1983).
6. Ch. Körber and M. W. Scheiwe, Observations on the non-planar freezing of aqueous salt solutions, *J. Crystal Growth* **61**, 307–316 (1983).
7. S. Kourosh, K. R. Diller and M. E. Crawford, Microscopic study of coupled heat and mass transport during unidirectional solidification of binary solutions—II. Mass transfer analysis, *Int. J. Heat Mass Transfer* **33**, 39–53 (1990).
8. S. Kourosh and K. R. Diller, A unidirectional temperature gradient stage for solidification in aqueous solutions, *J. Microscopy* **135**, 39–48 (1984).
9. C. D. Evans and K. R. Diller, A programmable, microprocessor controlled temperature stage for burn and freezing studies in the microcirculation, *Microvas. Res.* **24**, 214–225 (1982).
10. J. C. White and R. R. Miller, Densities and freezing points of sodium permanganate, *J. Am. Chem. Soc.* **75**, 3282–3283 (1953).
11. V. J. Lunardini, *Heat Transfer in Cold Climates*. Van Nostrand Reinhold, New York (1981).

ETUDE MICROSCOPIQUE DU TRANSFERT COUPLE DE CHALEUR ET DE MASSE PENDANT LA SOLIDIFICATION UNIDIRECTIONNELLE DE SOLUTIONS BINAIRES—I. ANALYSE THERMIQUE

Résumé—Les phénomènes couplés de transfert de chaleur et de masse pendant la solidification unidirectionnelle d'une solution binaire sont étudiés en utilisant un stage spécial du gel pour la microscopie à lumière transmise. L'appareil permet l'observation directe en temps réel du mécanisme de solidification avec mesure simultanée de l'échelle cellulaire des champs couplés de concentration et de température, avec leur interaction. Les données expérimentales fournissent une compréhension du processus de solidification au niveau microscopique utile aux modèles du mécanisme de solidification binaire, en incluant les profils temporels et spatiaux de température, les vitesses locales de refroidissement, les flux thermiques, la vitesse et la température à l'interface.

MIKROSKOPISCHE UNTERSUCHUNG DES GEKOPPELTEN WÄRME- UND STOFFTRANSPORTS BEI DER GERICHTETEN ERSTARRUNG BINÄRER LÖSUNGEN—I. UNTERSUCHUNG DES WÄRMETRANSPORTS

Zusammenfassung—Mit Hilfe einer speziellen Gefriereinrichtung für Durchlichtmikroskopie wurde der gekoppelte Wärme- und Stofftransport untersucht, der bei der gerichteten Erstarrung in binären Lösungen auftritt. Die Apparatur gibt die Möglichkeit der Echtzeitbeobachtung des Gefriervorgangs zusammen mit der gleichzeitigen Messung des zeitlichen Verlaufs der gekoppelten Mikrokonzentrations- und Temperaturfelder und deren gegenseitiger Beeinflussung. Die experimentellen Werte ermöglichen eine verständliche Beschreibung des Gefriervorgangs auf mikroskopischer Ebene, die zur Entwicklung binärer Erstarrungsmodelle sehr nützlich ist. Sie enthält räumliche und zeitliche Temperaturprofile, lokale Werte von Kühlgeschwindigkeit und Wärmestromdichte sowie Geschwindigkeits- und Temperaturentwicklung der Phasengrenze.

МИКРОСКОПИЧЕСКОЕ ИССЛЕДОВАНИЕ СВЯЗАННОГО ТЕПЛО- И МАССОПЕРЕНОСА В ПРОЦЕССЕ НАПРАВЛЕННОГО ЗАТВЕРДЕВАНИЯ БИНАРНЫХ РАСТВОРОВ—I. ТЕРМИЧЕСКИЙ АНАЛИЗ

Аннотация—С использованием специально сконструированного устройства для оптической микроскопии прозрачных сред исследуются явления связанного тапло- и массопереноса, происходящие при направленном затвердевании бинарного раствора. Установка обеспечивает непосредственное наблюдение за процессом замораживания в реальном масштабе времени с одновременным измерением эволюции взаимосвязанных концентрационного и температурного полей. Экспериментальные данные дают возможность получить исчерпывающую характеристику процесса замораживания на микроскопическом уровне для использования ее при разработке моделей процесса бинарного затвердевания, включая временной и пространственный температурные профили, локальные значения скорости охлаждения и теплового потока, а также скорость и температуру межфазной границы.